

HiSST: 4th International Conference on High-Speed Vehicle Science Technology 22 -26 September 2025, Tours, France



Numerical Analysis on Spray Characteristics of a Preheated Liquid Fuel Jet in Supersonic Crossflow

Donggyu Yun¹, Hyunwoo Kim², Hong-Gye Sung³

Abstract

The liquid fuel break-up and spray combustion in supersonic crossflow are primarily encountered in scramjet engines. In scramjet engines, the residence time for combustion is extremely short, requiring the fuel to vaporize and mix rapidly. A preheated liquid jet injector can be considered as the effective way to enhance the liquid break-up and atomize at certain time. Therefore, in this study, the feasibility of preheated jet injection is validated, and the analysis is subsequently extended by injecting preheated JP-10 into a supersonic combustor. The numerical approach aims to provide a comprehensive simulation of the processes of ligament and droplet breakup and atomization, employing the homogeneous mixture model (HMM) and large eddy simulation (LES). Also, numerical techniques are applied, including the Novel-Abel Stiffened Gas (NASG) state equation, Adaptive Mesh Refinement (AMR), evaporation and phase change models, and the Eulerian-Lagrangian (EtoL) transformation.

Keywords: Homogeneous Mixture Model, Preheated Liquid Jet in Supersonic Crossflow, Adaptive Mesh Refinement, Evaporation

Nomenclature

Latin

D – Diameter of injector

e – Specific internal energy

E_t – Specific total energy

F – Force

h - Enthalpy

h_{fg} - Latent heat

 \dot{m} – Mass flow rate

N – Number of droplets

L - Injector length

p – Pressure

q – Heat flux ratio

Q – Heat of reaction

S – Source term

t - Time

author(s)

T – Temperature

U_K – Reaction velocity of species k

Greek

 γ – Ratio of specific heat

 δ_{ii} – Kronecker delta

 λ – Conductivity

 μ – Viscous coefficient

 ρ – Density

 σ – Surface tension

 τ_{ij} – Viscous stress tensor

Superscripts

- Time difference

Subscripts

cri - Critical

i, j, ij – Spatial coordinate index

I – Liquid phase

sat - Saturation

v - Gas phase

HiSST-2025-0201 Page | 1 Numerical Analysis on Spray Characteristics of a Preheated Liquid Fuel Jet in Supersonic Crossflow Copyright © 2025 by

¹ Korea Aerospace University, Goyang Gyeonggi 412-791 Republic of Korea, 010donggyu@kau.kr

² Korea Aerospace University, Goyang Gyeonggi 412-791 Republic of Korea, hyunwoo5316@kau.kr

³ Korea Aerospace University, Goyang Gyeonggi 412-791 Republic of Korea, hgsung@kau.ac.kr

1. Introduction

Given their broad operating envelope for hypersonic flight, scramjet engines are expected to place increasing demands on robust supersonic combustor operation [1]. Efficient mixing of liquid fuels is pivotal to combustor performance, and prior studies have made significant progress on the underlying atomization and breakup processes. Study on liquid-fuel injection into supersonic crossflows has long combined experiments, theory, and computation. Under laminar conditions, Sallam et al. [2] identified Rayleigh-Taylor instability along the jet surface and derived a wavelength correlation expressed in terms of the Weber number, clarifying key breakup physics. Using nanoparticle planar laser scattering (NPLS), Sun et al. [3] refined a penetration depth correlation formulated around the momentum flux ratio, thereby improving measurement informed modelling. Hagen [4] compared penetration depth, breakup length, and jet-shock separation across laminar and turbulent regimes in supersonic crossflow injection. At lower temperatures, Yun et al. [5] employed a homogeneous mixture model to examine the influence of spray angle on breakup and atomization and coupled Lagrangian particles to propose empirical trends for penetration depth and Sauter Mean Diameter (SMD). Notably, most existing studies have used ambient-temperature, non-evaporating fuels, leaving a gap relative to high-temperature operational environments. Under continuous operation, thermal management of the airframe and engine components is required; routing the aircraft's own fuel through regenerative cooling passages provides the necessary heat removal while avoiding the mass penalty of dedicated coolant and heat exchanger systems. Active thermal management is expected to be central: liquid fuel can absorb heat in cooling channels and then be injected preheated, potentially approaching near-critical or even supercritical conditions, where evaporation becomes a dominant accompanying process [6,7]. Preheating accelerates atomization and vaporization, shortens the fuel-air mixing time, and enhances mixing quality, which collectively broadens extinction limits, aids ignition, and improves combustion efficiency. To quantify temperature effects, Yoo et al. [8] used a Lagrangian particle framework to evaluate droplet formation and proposed correlations for penetration and SMD as functions of temperature and momentum flux ratio, thereby extending predictive capability. Wang et al. [9] investigated the atomization and evaporation behaviour of kerosene for a rotating-detonation scramjet over a range of fuel temperatures. The results show that jet penetration depth is governed primary by fuel pressure and exhibits little dependence on fuel temperature. At present, few numerical studies have examined how injection temperature influences preheated JP-10. The atomization and evaporation behaviour of a preheated JP-10 liquid jet in a supersonic crossflow is investigated using a one type of governing equation homogeneous mixture model that treats compressible multiphase flow. To both limit computational expense and capture fine-scale breakup physics, adaptive mesh refinement and Eulerian-to-Lagrangian transformation are utilized.

2. Numerical method

2.1. Governing equation

The three-dimensional unsteady Navier-Stokes equations, utilizing the homogeneous mixture model, are discretized using the finite volume method. The governing equations depict the conservations of mass, momentum, energy, and chemical species in Cartesian coordinates, as shown in Eq. (1) through Eq. (4). The indices *i* and *j* represent spatial coordinates, while *k* denotes the index for different species.

$$\frac{\partial \rho}{\partial t} + \frac{\partial \rho u_i}{\partial x_i} = \dot{S}_c \tag{1}$$

$$\frac{\partial \rho u_i}{\partial t} + \frac{\partial \rho u_i u_j}{\partial x_j} = -\frac{\partial p}{\partial x_i} + \frac{\partial \tau_{ij}}{\partial x_j} + \dot{S}_M$$
 (2)

$$\frac{\partial \rho E}{\partial t} + \frac{\partial (\rho E_t + p) u_i}{\partial x_j} = -\frac{\partial q_j}{\partial x_j} + \frac{\partial u_i \tau_{ij}}{\partial x_j} + \dot{S}_E$$
(3)

$$\frac{\partial \rho Y_k}{\partial t} + \frac{\partial \rho u_j Y_k}{\partial x_j} = -\frac{\partial (\rho V_{ij} Y_k)}{\partial x_j} + \dot{S}_{S,K}$$
(4)

$$\tau_{ij} = \mu \left(\frac{\partial u_i}{\partial x_j} + \frac{\partial u_j}{\partial x_i} \right) - \frac{2}{3} \mu \frac{\partial u_l}{\partial x_l} \delta_{ij}$$
 (5)

HiSST-2025-0201 Page |

$$q_{j} = -\lambda \frac{\partial T}{\partial x_{i}} + \rho \sum_{k=1}^{N} h_{k} Y_{k} U_{k,j}$$
(6)

The viscous stress tensor (τ) and heat flux vector (q) for Newtonian fluid are defined as Eqs. (5) and (6), respectively. μ , λ , e, and h represent the viscosity coefficient, thermal conductivity, specific internal energy, and specific enthalpy, respectively. The source terms governing two-way Eulerian-Lagrangian coupling are formulated in Eqs. (7) and (10).

$$\dot{S}_c = \sum_{k=1}^{N_p} \dot{m}_{p,k} \tag{7}$$

$$\dot{S}_{M} = \sum_{k=1}^{N_{p}} (\dot{m}_{p,k} u_{p,k,i} + m_{p,k} F_{p,i})$$
(8)

$$\dot{S}_E = \sum_{k=1}^{N_p} \left(F_{p,i} u_{p,k,i} + \dot{m}_{p,k} \left(h_s + \frac{1}{2} u_{p,k,i}^2 \right) + \dot{Q}_s \right)$$
 (9)

$$\dot{S}_{S,K} = \sum_{k=1}^{N_p} \dot{m}_{p,k} \tag{10}$$

2.2. Equation of state

The Noble–Abel stiffened-gas (NASG) equation of state [10] is adopted, which is applicable to liquids and conveniently represents liquid and gas behaviour within a single formulation over a broad pressure–temperature range. These parameters of constant coefficients characterize the thermodynamic properties of the fluid. The term $(\gamma-1)/(v-b)$ accounts for thermal agitation, where (v-b) signifies the effect of strong repulsive short-range interactions between molecules associated with molecular motion in gases, liquids, and solids. The parameters for liquid JP10 are provided in Table 1. The temperature dependence of viscosity and surface tension is represented by empirical correlations in Eqs. (11) and (12) [11,12].

Table 1. The NASG EOS properties for the liquid JP10.

Liquid	γ	$c_v(J/kg\cdotK)$	b (m³/kg)	$p_{\infty}(kPa)$	Q (kJ/kg)
JP10	1.09	2393.0	6.81×10 ⁻⁴	175,100	-794.696

$$\mu_l = exp \left\{ \frac{1.824}{\frac{T}{273.15} - 0.43009} - 1.9945 \left(\frac{T}{273.15} \right) + 0.37044 \left(\frac{T}{273.15} \right)^2$$
 (11)

$$\sigma = 8.929 \cdot 10^{-9} T^2 - 9.862 \cdot 10^{-5} T + 5.929 \cdot 10^{-2}$$
 (12)

2.3. Phase change model

Phase change is modeled using the Lee model [13]. When the liquid temperature exceeds the saturation temperature, the volumetric evaporation rate is Eq. (13). When the vapor temperature is below saturation temperature, the condensation rate is Eq. (14). α_l and α_v are the phase volume fractions, ρ_l and ρ_v are the liquid and vapor densities. ξ_e and ξ_c denote the mass transfer intensity factor that set the characteristic phase-change time scale. The mass transfer intensity factor is an empirical coefficient whose value depends on the situation; consistent with common practice, a value of 0.1 is used in the present study. All the numerical schemes have been implemented and parallelized in an inhouse code MASCH (Multiphysics-All-Speeds CFD by HPCL) [14].

$$T_l > T_{sat}, \ \dot{m}_{lv} = \xi_e \alpha_l \rho_l \frac{T_l - T_{sat}}{T_{cat}}$$
 (13)

$$T_v < T_{sat}, \ \dot{m}_{vl} = \xi_c \alpha_v \rho_v \frac{T_{sat} - T_v}{T_{sat}}$$
 (14)

HiSST-2025-0201 Page | 3 Numerical Analysis on Spray Characteristics of a Preheated Liquid Fuel Jet in Supersonic Crossflow Copyright © 2025 by

3. Validation

Fig. 1(a) outlines the high temperature fuel injection setup and summarizes the diagnostics [15]. Fig. 1(b) depicts the expansion test section analyzed. A single circular injector is flush mounted at the center of the upper wall near the inlet, issuing a jet into the main flow. The inset highlights the interaction between the wall boundary layer and the jet shear layer at the injector lip. For the simulations, the computational domain covers the entire expansion section, including the injector, and adaptive mesh refinement is applied locally around the injector to resolve steep gradients. The injector orifice is 0.7 mm in diameter and 4.3 mm in length (L/D = 6.1) with a sharp-edged geometry. The mesh comprises 3.42 million cells. Subsonic inflow and outflow boundary conditions are imposed, and no-slip walls are applied in the vicinity of the injector. Three injection cases are considered at a pressure drop of 0.3 MPa with fuel temperatures of 433, 473, and 503K. The fuel is JP-10 (C10H16) with a boiling point of approximately 460K.

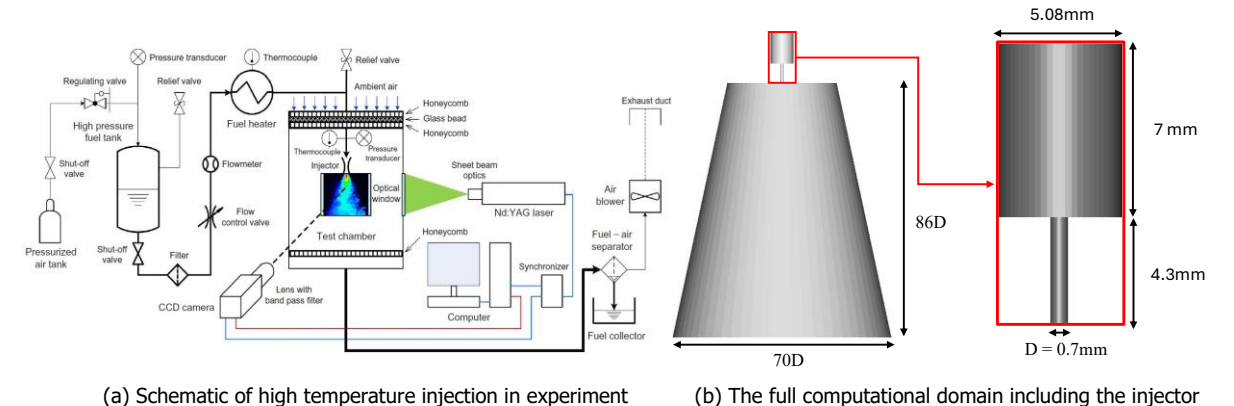


Fig 1. The experiment (a) [15] and computational domain (b) including the injector.

The influence of fuel injection temperature on spray characteristics is systematically examined through comparison of experimental visualization, averaged MIE scattering, and numerical simulation. At a lower injection temperature of 433 K (Fig. 2), the jet exhibited a slender, coherent structure with minimal lateral dispersion. Both MIE scattering and CFD predictions confirmed that the spray angle is scarcely formed, consistent with the experimentally observed straight jet trajectory. When the injection temperature was increased to 473 K (Fig. 3), the experimental results revealed enhanced breakup and radial spreading of the jet. At 503 K (Fig. 4), a pronounced widening of the spray angle is observed in both the experiment and MIE scattering, indicating accelerated atomization and evaporation processes. The trajectory of the mass fraction transformed into gas is indicated in red lines. The CFD simulation successfully replicated the global spray expansion, and a quantitative comparison of spray angles at X/D=5 (Fig. 5) demonstrated that the numerical predictions followed the same increasing trend as the experiments.

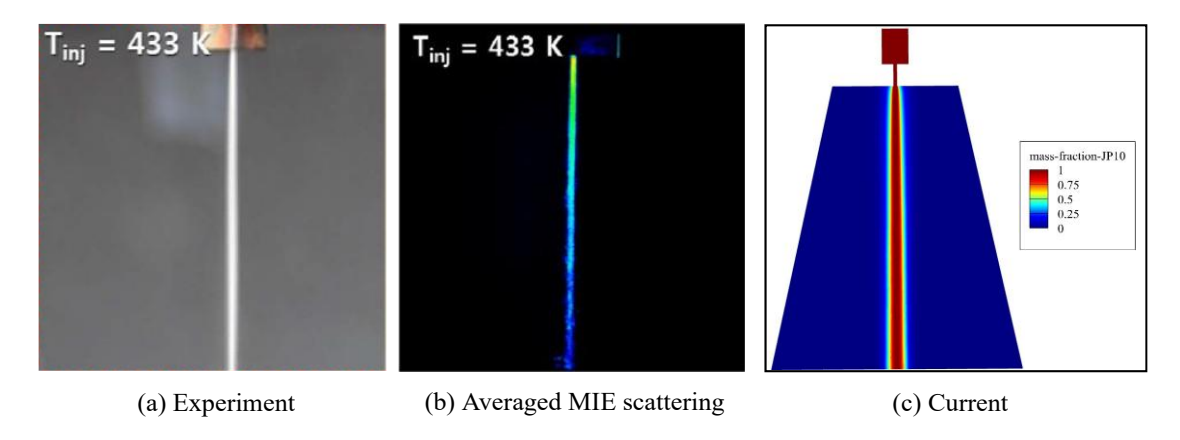


Fig 2. Fuel injection according to fuel temperature, T_{ini} =433K.

HiSST-2025-0201 Page | Copyright © 2025 by author(s)

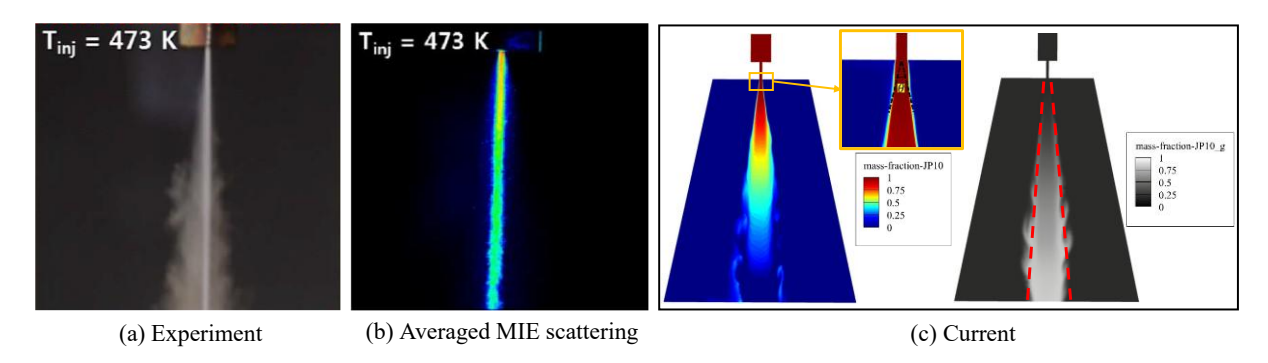


Fig 3. Fuel injection according to fuel temperature, T_{inj} =473K.

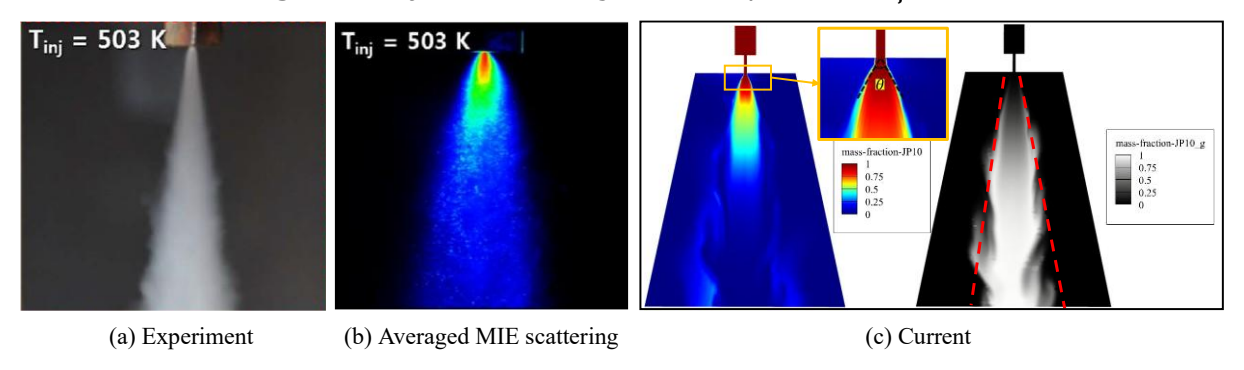


Fig 4. Fuel injection according to fuel temperature, T_{ini} =503K.

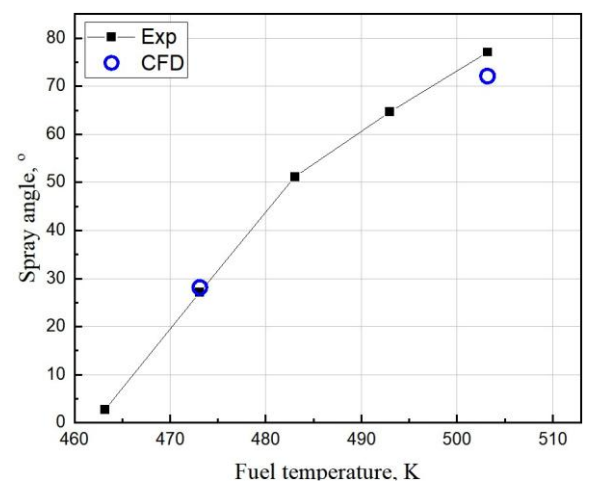


Fig 5. Spray angle at X/D = 5 according to fuel temperature.

4. Results and discussion

A schematic of the wind-tunnel facility is shown in Fig. 6(a), and the computational domain around the injector is presented in Fig. 6(b). The injector diameter (D) is 0.7mm. The three-dimensional domain extends over [0.0D, 280.0D]×[0.0D, 40.0D]×[0.0D, 40.0D] with a 15° expansion angle. The liquid fuel injector is located 20D downstream of the inlet plane. Supersonic inflow and outflow boundary conditions are applied, while the top and bottom surfaces are treated as no-slip walls. The inlet velocity profile is taken from measurements of fully developed flow, and the crossflow Mach number is set to 2.0.

HiSST-2025-0201 Page | 5 Numerical Analysis on Spray Characteristics of a Preheated Liquid Fuel Jet in Supersonic Crossflow

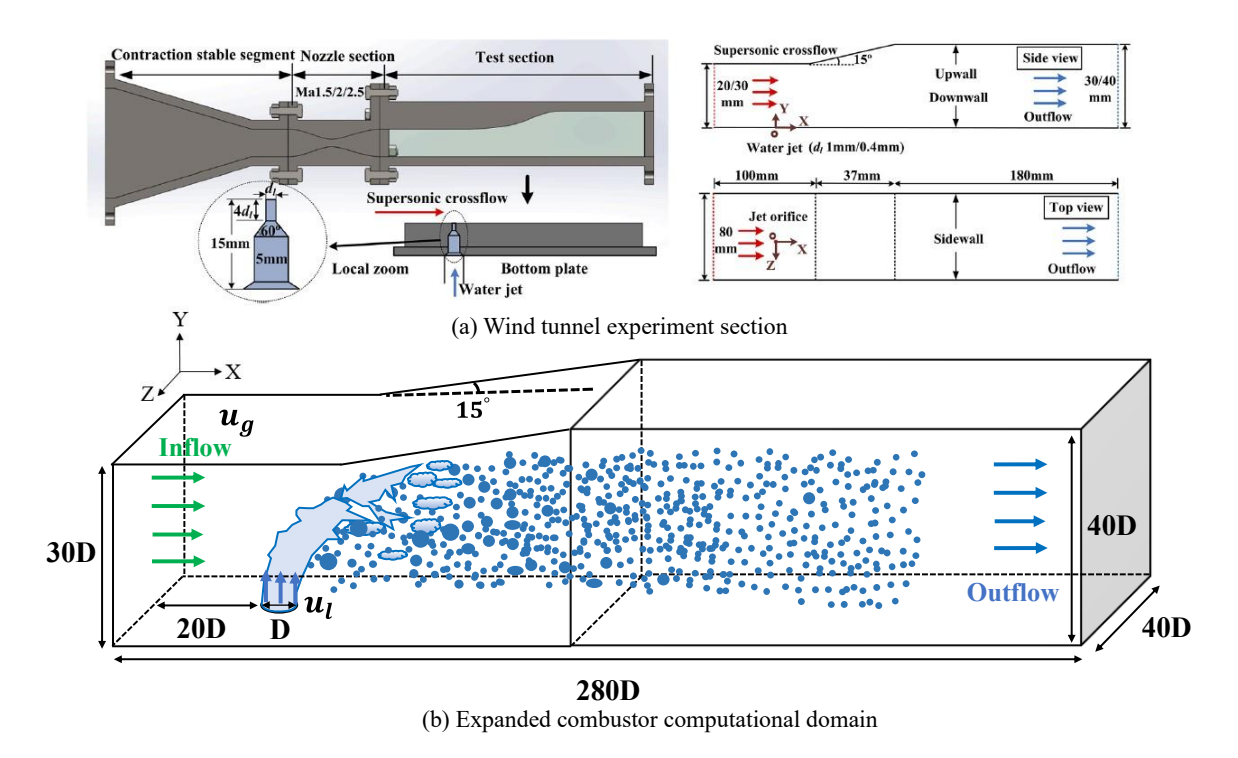


Fig 6. Schematics of wind tunnel experiment section (a) and computational domain (b).

In a jet in supersonic crossflow, a bow shock forms ahead of the jet at the inflow, and shock—shear interactions generate an upstream separation bubble and a strong shear layer in which Kelvin—Helmholtz instability rapidly fragments the liquid core into ligaments and droplets. In the near field breakup is dominant, whereas farther downstream evaporation and dilution prevail, producing a thick vapor plume and increasing the cross-sectional temperature and scalar fluctuations. Moreover, the fuel column does not remain as a single liquid phase but appears as a liquid—vapor mixture; to resolve the phase interface, AMR is employed as depicted in Fig. 7. The mixing and evaporation behaviour of JP-10 injected at a constant mass flow rate is examined while the injector-exit temperature is raised from 473, 503 to 533K. In the liquid phase mass fraction fields as shown in Fig. 8, the JP-10 distribution illustrates the behaviour of the liquid phase in the supersonic crossflow. As the fuel temperature rises, the viscosity, surface tension, and density decrease, advancing the onset of breakup and shortening the breakup length; at the same time the evaporation rate increases, thereby reducing the local liquid fraction. For the gas phase JP-10 mass fraction, the plume remains as localized patches near the exit at 473K, becomes a continuous vapor plume at 503K, and at 533K thickens and covers a large area, persisting much farther downstream as depicted in Fig. 9.

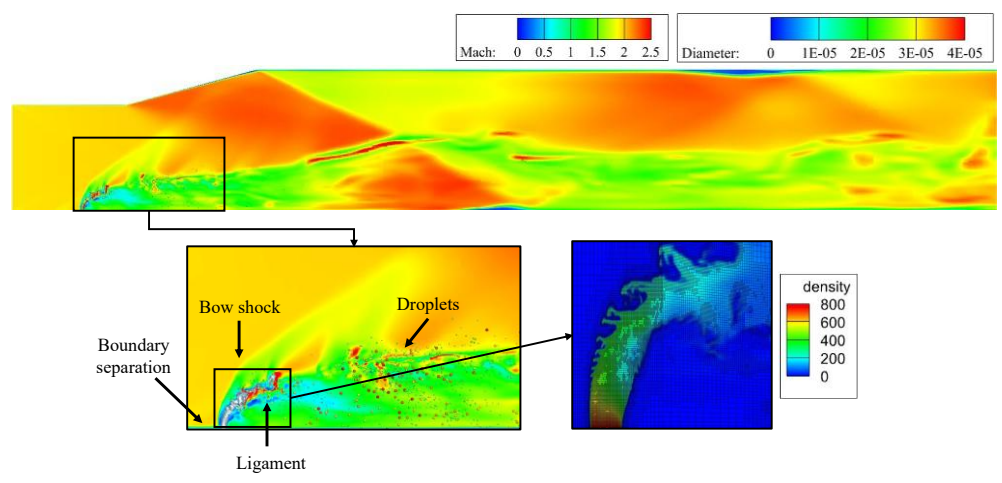


Fig 7. Physical phenomena around the liquid jet and evolution of AMR levels.

HiSST-2025-0201 Page | 6

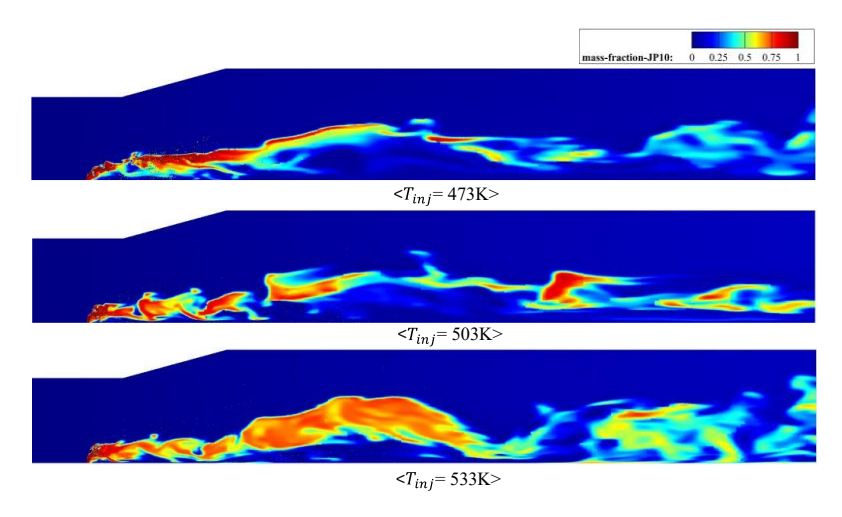


Fig 8. The liquid mass fraction distribution of JP-10 to injection temperature.

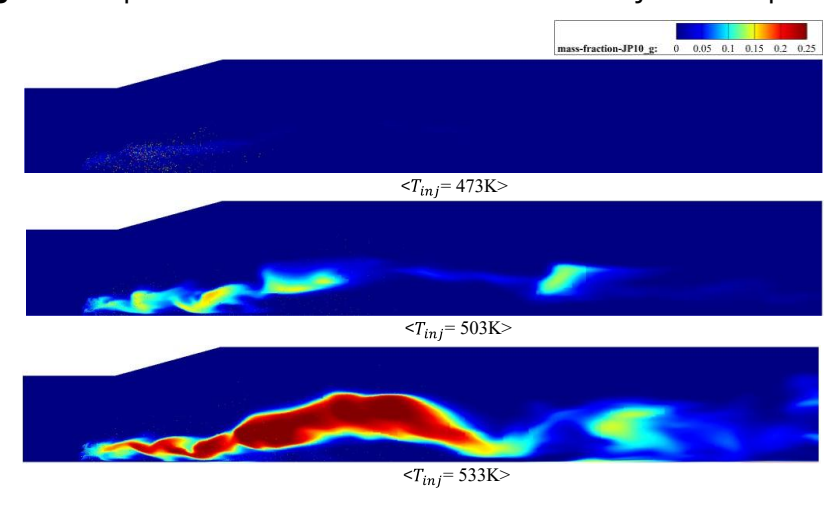


Fig 9. The gas mass fraction distribution of JP-10 to injection temperature.

Fig. 7 shows the streamwise variation of static temperature. Increasing the injection temperature does not change the qualitative trend; the temperature is generally higher under the high-temperature condition, and the peak occurs at the orifice. The pronounced local variations are caused by the bow shock produced by the liquid jet and by the expansion waves and oblique shocks generated in the enlarged combustor section.

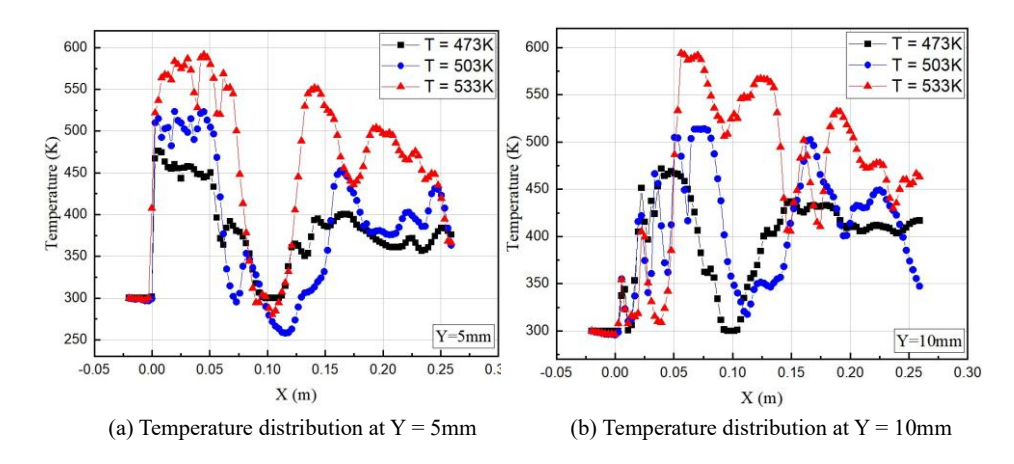


Fig 10. Temperature distribution according to X-axis.

As the fuel temperature rises, the liquid viscosity, surface tension, and density decrease, which increases the growth rate of interfacial instabilities; in other words, the Weber number increases, leading to faster breakup, a shorter breakup length, and a wider spray angle as shown in Fig. 11. In the region impinged by the crossflow, breakup occurs, whereas evaporation dominates elsewhere. Moreover, if the injection temperature exceeds the saturation temperature, flashing (explosive boiling) occurs, promoting breakup and atomization so that the liquid core vanishes rapidly, thereby enhancing downstream mixing and evaporation. Fig. 12 shows the x-vorticity distributions and sectional circulation at different injector-exit temperatures. The positive and negative circulations Γ_{\perp} and Γ_{-} are obtained by integrating vorticity over regions with positive and negative sign, and the pair strength is $\Gamma_{pair} =$ $\Gamma_{+} + \Gamma_{-}$. As the injection temperature increases, the circulation-based pair strength Γ_{pair} rises by approximately 23% when the temperature is raised from 473K to 503K and by 48% when raised from 503K to 533K, corresponding to an overall increase of about 81% between 473K and 533K; this indicates a marked strengthening of the counter-rotating vortex pair and in turn, enhanced entrainment and mixing.

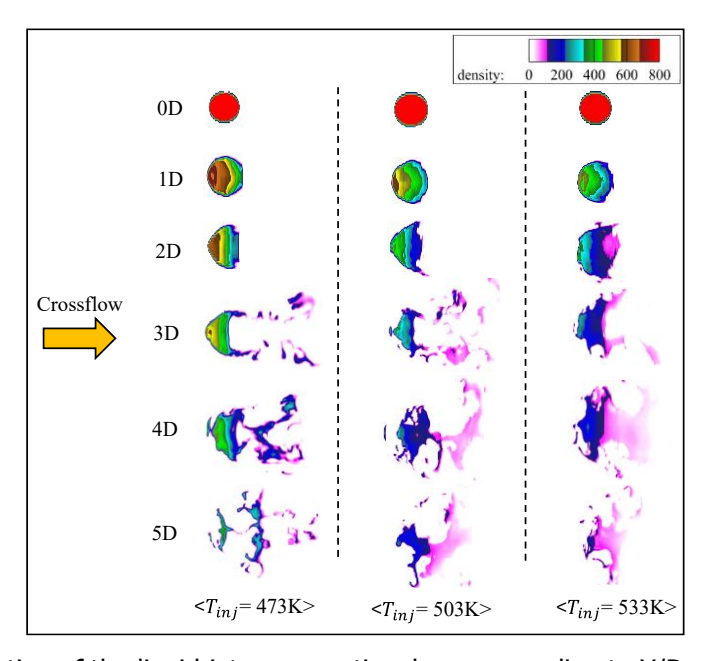


Fig 11. The variation of the liquid jet cross sectional area according to Y/D = 0,1,2,3,4 and 5.

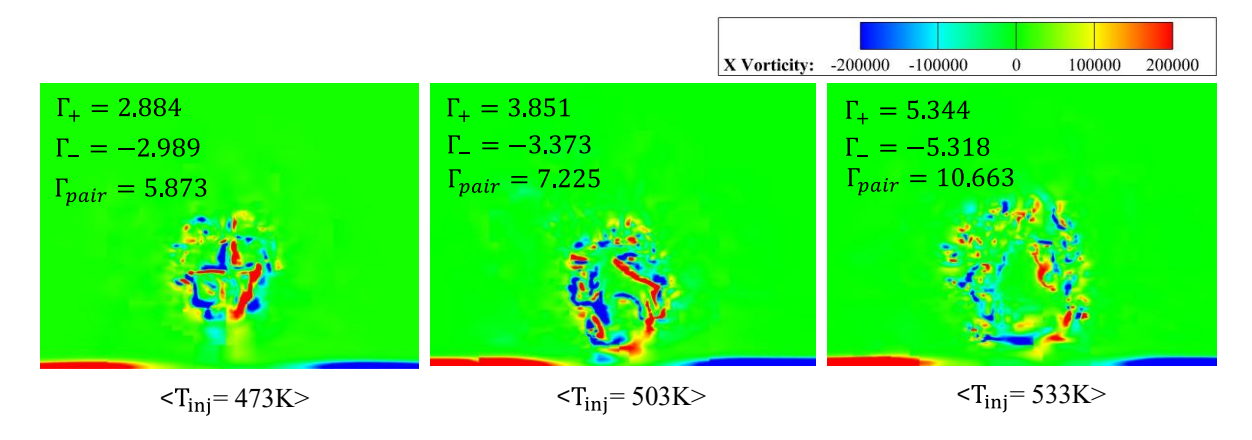


Fig 12. X-vorticity distribution with vortex-rotation vectors and magnitudes at X/D = 5.

HiSST-2025-0201 Page | Copyright © 2025 by author(s)

5. Conclusion

A compressible multi-phase large eddy simulation, inhouse code, is developed and conducted to investigate the evaporation of the preheated liquid JP-10 jet in supersonic crossflow. The governing equations, which utilize the homogeneous mixture model, are expressed in general forms, and the equation of state is capable of simulating both gas and liquid phases. To conduct a detailed analysis, AMR and EtoL transformation are implemented near the interface between the phases. Accordingly, the evaporation of preheated JP-10 injected from a manifold injector is simulated and validated. In supersonic crossflow with preheated JP-10 injection, a multiphase simulation stably resolved the liquidgas interface and quantitatively characterized the breakup and evaporation processes governed by the bow shock, shear layer, and counter-rotating vortex pairs. The liquid mass fraction decayed more rapidly while the vapor plume became continuous and more voluminous, persisting farther downstream. Breakup dominated in the region directly impinged by the crossflow, whereas evaporation prevailed elsewhere; when the injection temperature exceeded the saturation temperature, flashing (explosive boiling) further accelerated atomization, leading to rapid disappearance of the liquid core and enhanced downstream mixing and evaporation. Sectional integration of the X-vorticity showed that the pair strength increased by about 81% overall between 473K to 533K, quantitatively confirming that fuel heating significantly strengthens entrainment and mixing.

References

author(s)

- 1. Urzay, J.: Supersonic Combustion in Air-Breathing Propulsion Systems for Hypersonic Flight. Annual Review of Fluid Mechanics. 50, 593–627 (2018)
- 2. Sallam, K.A., Aalburg, C., Faeth, G. M.: Breakup of Round Nonturbulent Liquid Jets in Gaseous Crossflow. AIAA Journal. 42(12), 2529-2540 (2004)
- 3. SUN, M.B., Zhang, S. P., Zhao, Y. H., Zhao, Y.X., Liang, J.H.: Experimental investigation on transverse jet penetration into a supersonic turbulent crossflow. Science China Technological Sciences. 56, 1989-1998 (2013)
- 4. Hagen, W. A.: Numerical modelling of liquid jets in crossflow with applications to supersonic combustion ramjets, Thesis and Dissertations, Iowa State University, USA (2017)
- 5. Yun, D. G., Yoo, Y. L., Sung, H. G.: High-fidelity simulation of angled liquid jet breakup in supersonic crossflow. Aerospace Science and Technology. 163, 1-19 (2025)
- 6. Gao, Y., Zhang, C., Jing, H., Tong, Y., Lin, Z.: Characteristics of Transverse Liquid Jets at Different Preheated Temperature in Supersonic Crossflow. Applied Thermal Engineering. 279(15), 1-15 (2025)
- 7. Feng, G., Zhang, J., Hu, Z., Luan, G., Wang, Y., Bao, W.: Investigation on diffusion and mixing characteristics of liquid kerosene with phase change under different inflow conditions. Acta Astronautica. 236, 869-881 (2025)
- 8. Yoo, Y. L., Han, D. H., Hong, J. S., Sung, H. G.: A large eddy simulation of the breakup and atomization of a liquid jet into a cross turbulent flow at various spray conditions. International Journal of Heat and Mass Transfer. 112, 97-112 (2017)
- 9. Wang, J., Lin, W., Huang, W., Shi, Q., Zhao, J.: Numerical study on atomization and evaporation characteristics of preheated kerosene jet in a rotating detonation scramjet combustor. Applied Thermal Engineering. 203, 1-13 (2022)
- 10. Metayer, O., Saurel, R.: The noble-abel stiffened gas equation of state. Physics of Fluids. 28, 1-34 (2016)
- 11. Lee, H. J., Choi, H. J., Hwang, G. Y., Park, D. C., Min, S. K.: Numerical study of choked cavitation in high temperature hydrocarbon liquid jets. International Journal of Heat and Fluid Flow. 68, 114-125 (2017)
- 12. Lee, H. J., Jin, Y. I., Choi, H. J., Hwang, K. Y.: Hydraulic characterization of high temperature hydrocarbon liquid jets. International Journal of Heat and Fluid Flow. 65, 166-176 (2017)

- 13. Holesova, N., Lenhard, R., Kaduchova, K., Malcho, M.: Correlation Coefficients in Lee's Model of Multiphase Flows. MATEC Web of Conference 369, 1-9 (2022)
- 14. Yun, D. G., Sung, H. G.: Detailed analysis on primary and secondary break up characteristics of liquid fuel jet in crossflow using homogeneous mixture model and large eddy simulation. Physics of Fluids. 36, 1-20 (2024)
- 15. Jin, Y. I., Lee, H. J., Hwang, G. Y., Park, D. C., Min, S. K.: Flashing injection of high temperature hydrocarbon liquid jets. Experimental Thermal and Fluid Science. 90, 200-211 (2018)

HiSST-2025-0201 Page | 10